DOI: 10.1590/2317-4889201620160101

ARTICLE

The Piriá aluminous lateritic profile: mineralogy, geochemistry and parent rock

O perfil laterítico aluminoso do Piriá: mineralogia, geoquímica e rocha mãe

Pabllo Henrique Costa dos Santos[1]*, Marcondes Lima da Costa[2], Alessandro Sabá Leite[3]

ABSTRACT: Relatively small aluminous lateritic deposits are abundant in the northeast and northwest parts of the Pará and Maranhão states, respectively. Most of them hosts aluminum phosphate mineralization forming hills and plateaus that stand out in the topography of the undulating plains of this region. The Piriá ridge is one of those topographic features, covered by lateritic iron crusts that have been studied in the 1970s as part of iron ore exploration campaigns and recently for phosphates prospection. This study improves the knowledge about the evolution of the lateritic Piriá deposit and demonstrates its relationship with the most evolved laterites of the Amazon, known as mature laterites, which formed major ore deposits during the Paleogene. Samples of a 17 meter-deep borehole were investigated through mineralogical (X-ray diffraction —XRD, optical and electron microscopy) and chemical methods (inductively coupled plasma mass spectrometry — ICP-MS, inductively coupled plasma optical emission spectrometry — ICP-OES and X-ray fluorescence — XRF). The studied lateritic profile comprises a clay bauxitic horizon overlaid by an aluminous iron crust. Upwardly continuous dissolution of kaolinite occurs with the formation of gibbsite, as the result of intensive leaching, resulting in a higher Al2O3 content in the crust. The continuous formation of hematite from goethite resulted from the transition to more arid conditions. Anatase is a newly formed mineral (100–400 nm crystallites), showing a gradual increase, following the increase in TiO2 content, which is high and indicative of a mafic parent rock, confirmed by the Ti × Zr dispersion pattern. Prominent zoning in the lateritic profile is characterized by the mineralization in bauxite and augelite and abrupt chemical transition between the horizons, marked by a decrease in Si and increase in Fe content from the bottom to the top of the profile. These features are compatible and indicative of mature laterites formed in Amazon during the Paleogene.

KEYWORDS: Gurupi region; mature laterites; bauxite.

RESUMO: *Depósitos lateríticos de pequeno porte são frequentes no nordeste do Pará e noroeste do Maranhão. A maioria está mineralizada em fosfatos de alumínio e ocorre em morros e platôs, que se destacam na planície rebaixada dessa região. A Serra do Piriá é uma dessas feições, estando recoberta por couraças ferruginosas, alvo de explotação na década de 1970 e de recente prospecção de fosfatos. Este trabalho buscou aprofundar o conhecimento sobre a evolução laterítica do depósito Piriá e demonstrar sua compatibilidade com os lateritos mais evoluídos da Amazônia, conhecidos como maturos, os quais constituem grandes mineralizações formadas durante o paleógeno. Investigaram-se amostras de um furo de sondagem com 17 m de profundidade, por meio de análises mineralógicas (difração de raios x — DRX, microscopia ótica e eletrônica) e químicas (espectrometria de massa por plasma acoplado indutivamente — ICP-MS, espectrometria de emissão óptica com plasma indutivamente acoplado — ICP-OES e espectrometria de fluorescência de raios X — FRX). O perfil compreende horizonte argiloso bauxítico recoberto por crosta ferroaluminosa. Ascendentemente ocorre contínua dissolução da caulinita com formação de gibbsita, resultante de intensa lixiviação, de modo que os teores de Al2O3 são superiores na crosta. Também se verificou contínua formação de hematita a partir de goethita, resultante de transição para condições mais áridas. Anatásio neoformado (em cristalitos de 100 a 400 nm) apresenta maior abundância em direção ao topo, acompanhando os teores de TiO2, que são elevados e remetem à rocha mãe, de composição máfica, confirmada pelo padrão de dispersão Ti × Zr. A mineralização em bauxita e augelita e a transição composicional brusca entre os horizontes, principalmente quanto aos teores decrescentes de Si e crescentes de Fe em direção ao topo, demonstram o forte zoneamento típico dos lateritos maturos, formados na Amazônia durante o paleógeno.*

PALAVRAS-CHAVE: *região do Gurupi; lateritos maturos; bauxita.*

[1]Geosciences Museum, Institute of Geosciences, Federal University of Pará – UFPA, Belém (PA), Brazil. *E-mails: phsantos@ufpa.br, pabllo-santos@hotmail.com*

[2]Program for Post-graduation in Geology and Geochemistry, Institute of Geosciences, UFPA, Belém (PA), Brazil. *E-mails: mlc@ufpa.br, marcondeslc@gmail.com*

[3]Vale Institute of Technology – ITV, Belém (PA), Brazil. *E-mails: alessandro.leite@me.com, alessandroleite@oi.com.br*

*Corresponding author.

Manuscript ID: 20160101. **Received in:** 08/17/2016. **Approved in:** 09/23/2016.

INTRODUCTION

Lateritic deposits are found in almost the entire Amazon region. Among the main identified Amazonian lateritic zones, the Gurupi region (northeastern Pará and northwestern Maranhão, extending until the coast) stands out for its compositional diversity and metallogenic potential, mainly for phosphates, manganese, gold, titanium and aluminum (Costa 1997). In previous years, geological exploration for phosphates has intensified because of the Brazilian demand for fertilizers, which depends on large-scale imports. Primary and secondary gold searches continue to occur.

Most of the lateritic deposits from the Gurupi region are classified as mature. This term represents evolved laterites with more individualized and complex horizons, recognized by typical textures, structures and mineral-geochemical aspects (Costa 1991). Generally, these deposits comprise higher relief in the form of hills or ridges that stand out in the regional undulating plain.

The Gurupi region's main lateritic deposits, which host phosphate mineralization and are sometimes associated with bauxite, include the Sapucaia, Boa Vista, Jandiá, Cansa Perna, Itacupim, Pedra Grande, Piriá and Peito de Moça (in the state of Pará); and the Pirocaua, Trauira and Tromaí (in the state of Maranhão) (Fig. 1A). The most significant deposits in terms of volume and P_2O_5 content are the Sapucaia (that recently began to be mined) (Leite 2014), Itacupim, Pirocaua and Trauira (Oliveira & Costa 1984).

Physiographic and geological context

Piriá ridge is located along the left border of the homonymous river, in the municipality of Vizeu, northeastern Pará. The ridge comprises a chain of N–S-oriented plateaus, which are 6 km-long in length and 178 m high, near the border of

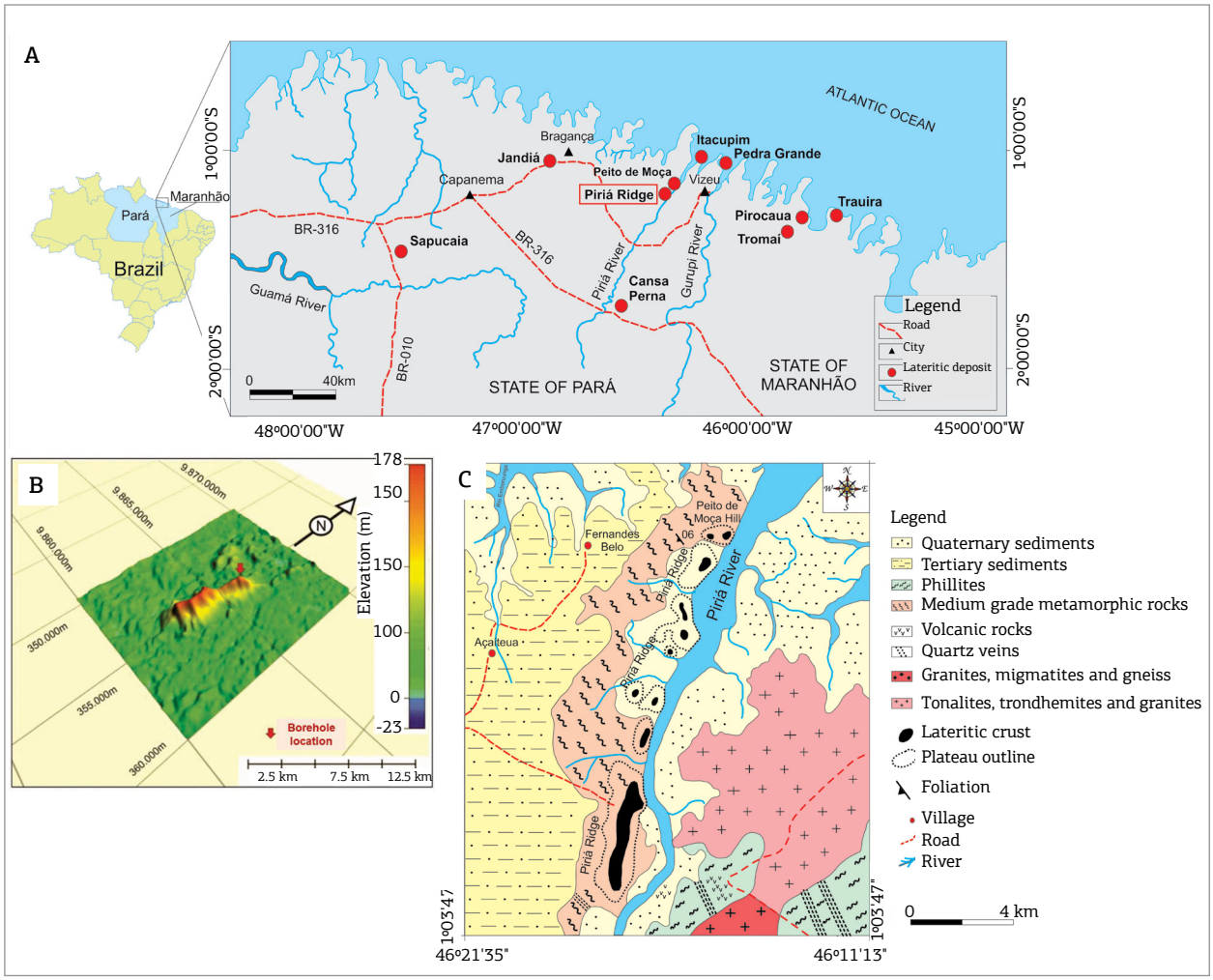

Figure 1. (A) Phosphate and bauxite deposits located along the coast of northeastern Pará and northwestern Maranhão, with Piriá ridge highlighted (Costa & Sá 1980, Costa 1980; Costa 1990, Costa 1997); (B) three-dimensional Piriá ridge, generated with Global Mapper 14 software from digital elevation model (Shutte Radar Topography Mission); (C) Piriá ridge and its surrounding geology, modified from Costa (1982).

Piriá river (Fig. 1B). The overlaying aluminous iron crust was partially mined during the 1980s and 1990s by Cimentos do Brasil S/A (CIBRASA) as iron ore, added to the limestone that was extracted near Capanema (Pará) to produce cement. The altitude in the area of exploitation was 160 m.

The ridge relief is sustained by lateritic crusts. Phyllite, schist and local volcanic rocks and quartz veins outcrop along the ridge slopes (Fig. 1C). This lithotype association matches the Aurizona Group, which was defined by Pastana (1995) as a greenschist to amphibolite facies meta-volcanosedimentary sequence that comprises various schists, phyllites, meta-pyroclastic rocks, meta-chert and some meta-mafic and meta-ultramafic rocks. Klein and Moura (2001) defined 2240 ± 5 Ma as the age for this unit.

Granites, granodiorites and trondhjemites also occur around Piriá ridge. These rocks match the Tromaí intrusive suite (Klein *et al.* 2005), which has great geographic extension and comprises batholiths of tonalites, trondhjemites, granodiorites and subordinate monzogranites. The Rb-Sr and K-Ar ages are 2076 ± 96 Ma and 1945 ± 90 Ma, respectively (Klein *et al.* 2005).

MATERIALS AND METHODS

Field work

The samples were acquired from Vicenza Mineração S/A. The company has prospected phosphates in the Gurupi region, and the Piriá ridge has been one of its targets. A 17 m-deep borehole was drilled at the top of the northern part of the ridge (coordinates 1º12'49"S/46º17'42"W). The motorized mechanical drilling method fragmented the samples used in this study. The drill core was logged in detail and 34 samples were collected at every 0.5 m interval.

The samples were labeled, described, photographed and classified. Afterward, they were homogenized, quartered and a 15 g aliquot was sprayed in an agate mortar for X-ray diffraction (XRD) and bulk rock chemical analysis. Other *in natura* samples were employed for the production of ten polished thin sections.

Mineral and morphological analyses

XRD and optical microscopy analysis were conducted. The XRD analysis identified the mineral contents of 17 selected samples by using the powder diffraction method with a diffractometer PANalytical X' PERT PRO MPD (PW 3040/60), goniometer PW 3050/60 (theta-theta) with a copper anode. The results were treated with the X'Pert High Score Plus software, which compares the obtained peaks with those from the International Center on Diffraction Data (ICDD).

The optical microscopy analyses were conducted with a Zeiss microscope, Axio Lab Pol model, to determine the textural and some mineral aspects from the lateritic profile. The adopted nomenclature for the texture was that proposed by the *Atlas of Micromorphology of Mineral Alteration and Weathering* (Delvigne 1999). The mineral and textural aspects were captured with a Canon digital camera, model A460.

The Fe-Al substitution in FeOOH-AlOOH (goethite-diaspore) solid solution was determined according to Thiel's (1963) method, which evaluates the positioning variations of d_{111}, d_{130}, d_{140} and d_{021} goethite reflections according to the AlOOH molar content.

Anatase is a typical lateritic mineral (Costa *et al.* 1991, Oliveira *et al.* 2013, Giorgis *et al.* 2014), also present in Piriá ridge deposit. So there was an attempt to make a more advanced morphological description of anatase crystals as they occur in laterites, despite the small size. First of all, anatase crystallites were extracted and concentrated by Sayin and Jackson's (1975) method, which treats the samples with hexafluorotitanic acid (H_2TiF_6), that dissolves kaolinite and most of phyllosilicates and Al-hydroxides (such as gibbsite) in lateritic materials and related soils.

Anatase crystallites, if present (in this case, the bulk sample diffractograms indicate the occurrence of anatase), are concentrated in the residual, along with some rutile, zircon and iron oxide-hydroxides. Next, the iron oxide-hydroxide was eliminated with sodium dithionite-citrate-bicarbonate (DCB), according to Mehra and Jackson's (1960) method. Afterward, only anatase and zircon (which is rare) were present in the residual. The concentrates were analyzed by XRD, scanning electron microscopy (SEM) and energy dispersive spectrometry (EDS) with a LEO 1525 SEM, WD 6 mm, signal A inLens at the *Zentrum für Werkstoffanalytik Lauf* (ZWL), in Germany.

Chemical analysis

Thirteen samples were selected and submitted for bulk rock chemical analyses (major, minor and trace elements). The methods applied were inductively coupled plasma optical emission spectrometry (ICP-OES) and inductively coupled plasma mass spectrometry (ICP-MS) with fusion opening (which used lithium metaborate/tetraborate) and digestion with dilute nitric acid.

For precious and base metals (Au, Ag, As, Bi, Cd, Cu, Hg, Mo, Ni, Pb, Sb, Se, Tl, Zn), the digestion was conducted with royal water. The loss on ignition (LOI) was determined by 1,000ºC calcination. The major elements were determined by ICP-OES and the trace and Rare Earth Elements (REE) by ICP-MS. These analyses were held at Acme Analytical Laboratories Ltd., in Canada.

The present work also used the results of chemical analyses on 32 samples at Geosol Laboratórios Ltda., which were granted by the Vicenza Company. The major elements were determined by X-ray fluorescence (XRF) — tablet obtained with lithium tetraborate fusion —, the trace elements were determined by ICP (after multi-acid digestion), and the LOI was determined by 1,000ºC calcination. The following elements were determined through these methods: SiO_2, Al_2O_3, Fe_2O_3, CaO, TiO_2, P_2O_5, MnO (XRF); Ag, As, Ba, Co, Cu, Ga, Hf, Hg, Mo, Nb, Ni, Pb, Sb, Sc, Sn, Sr, Ta, Th, U, V, W, Y, Zn, Zr, La, Ce, Pr, Nd, Sm, Eu, Gd, Tb, Dy, Ho, Er, Tm, Yb and Lu (ICP-MS).

The results were treated with Excel 2010, in which a correlation matrix was prepared. Pairs of chemical elements with elevated correlation coefficients were selected to prepare binary dispersion diagrams of $Fe_2O_3 \times TiO_2$, $Al_2O_3 \times TiO_2$, $Fe_2O_3 \times V$, $Fe_2O_3 \times As$, Nb × Ta, Zr × Nb, Zr × Ta, Zr × Hf, $TiO_2 \times$ REE, and Zr × REE. The ternary diagram $Fe_2O_3 \times SiO_2 \times Al_2O_3$ allowed the samples to be classified according to the lateritic evolutionary grade (Bardossy 1982, Aleva & Creutzberg 1994). The REE were normalized by Evensen *et al.* (1978) chondrites and were presented in specific diagrams to demonstrate their distribution patterns. Finally, stoichiometric mineral quantification was carried out based on the chemical composition.

RESULTS

Piriá lateritic sequence of horizons

The Piriá sequence consists of a bauxitic clay horizon at the base (ranging from 7 to 17 m deep), covered, over rough contact, by an aluminous iron crust (from 7 m deep to the surface). The most outstanding feature is the color contrast among the horizons: ocher yellow in the bauxitic clay horizon (changing to a roseate between 15 and 17 m) and reddish brown in the aluminous iron crust (changing to dark brown in the shallowest 0.5 m because of organic matter accumulation near the surface) (Fig. 2).

Kaolinite, gibbsite, goethite and anatase are the main minerals in the bauxitic clay (Figs. 3A and 3B); goethite, hematite, gibbsite and anatase are the main minerals in the aluminous iron crust (Figs. 3C and 3D). Quartz, augelite and zircon are accessories in both horizons. Quartz was identified by optical microscopy; zircon, by the Zr content, which ranged between 250 and 380 ppm; and augelite was indicated by XRD with the use of X'Pert High Score Plus software and also confirmed by P_2O_5 contents, which reached 0.72%, four times larger than the 0.17% crustal average. The results agree with those of Costa (1982), who identified the same main phosphate, augelite, and also crandallite and variscite on Piriá ridge.

The investigated horizons show distinct mineral composition (Fig. 3E). The presence of kaolinite characterizes the bauxitic clay horizon; its content decreases towards the overlying aluminous iron crust horizon in which the clay mineral is absent in the XRD analysis. The hematite, goethite, gibbsite and augelite contents increase upwards.

The anatase content increases upward the profile and is generally above the crustal average, varying from 0.6 up to 5.7%. Most lateritic profiles show this increase in the anatase content. However, considering the low TiO_2 stability, these oscillations reflect the compositional heterogeneity of the parent rock. The concentrate of anatase shows crystallite aggregates with tendency to prismatic bipyramidal forms and individual sizes ranging from 100 up to 400 nm, as observed by SEM (Fig. 4A-D) and confirmed by XRD (Figs. 4E) and EDS (Fig. 4F).

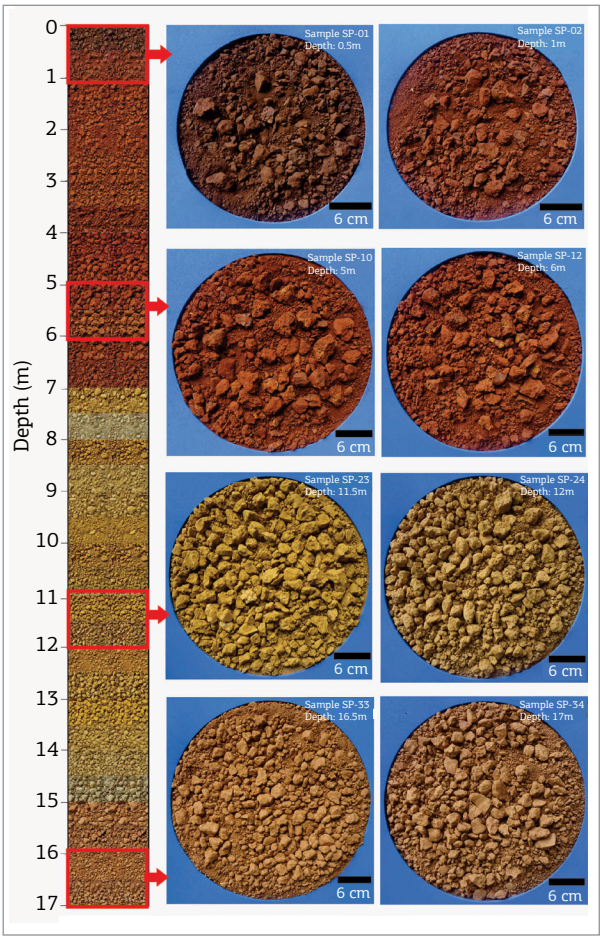

Figure 2. Textural and color aspects from the lateritic profile, which highlight the rough transition between the bauxitic clay and the aluminous iron crust.

Macro and micromorphology

Bauxitic clay horizon

The bauxitic clay horizon (Fig. 5A) comprises nodular compact blocks that are 0.5 to 4.0 cm in diameter and range from ocher yellow to pale yellow (Fig. 5B). These blocks are surrounded by ocher yellow to locally mottled sandy clay matrix (Fig. 5C), which also has smooth relict foliation (Fig. 5D), suggesting schistose parent rock.

Petrographic analysis, determined the general features of the bauxitic clay horizon as comprised of kaolinitic and subordinated gibbsitic matrix, involving micronodules and/or goethite and gibbsite or just gibbsite fragments. Gibbsite occurs in the matrix (associated with kaolinite) and as micronodules, both formed of microcrystalline gibbsite (Fig. 5E). The third group of gibbsite comprises mesocrystals and displays albite type twinning, mainly located in the dissolution cavities of the matrix (Fig. 5F).

The goethite constituted plasm that spotted the cryptocrystalline kaolinitic and gibbsitic crystals, giving yellowish and brownish tones to the matrix (Fig. 5G). This kaolinite cement was compact, but exhibited local smooth lamination (Fig. 5H) with yellowish and brownish bands, which reflect the variable goethite content, and other sub-translucent bands where kaolinite and gibbsite dominated.

Kaolinite, which was detected only in the bauxitic clay, was analyzed in terms of vertical variation on structural order/disorder. According to Amigó *et al.* (1994), this property modifies the Full Width at Half Maximum (FWHM) of 002 and 001 reflections obtained by XRD, which are located at 12°2θ and 25°2θ, respectively (Cu anode), and also modifies their asymmetry. Unlike most of lateritic deposits, no significant variation in the kaolinite structure was identified along the bauxitic clay horizon, possibly because of the relatively short sampling interval, but generically the kaolinite that composes the clay matrix tends to present high level of structural order, as shown by FWHM ranging from 0.13 to 0.18°2θ for the 001 plain and from 0.13 to 0.17 for the 002 plain (Fig. 6)

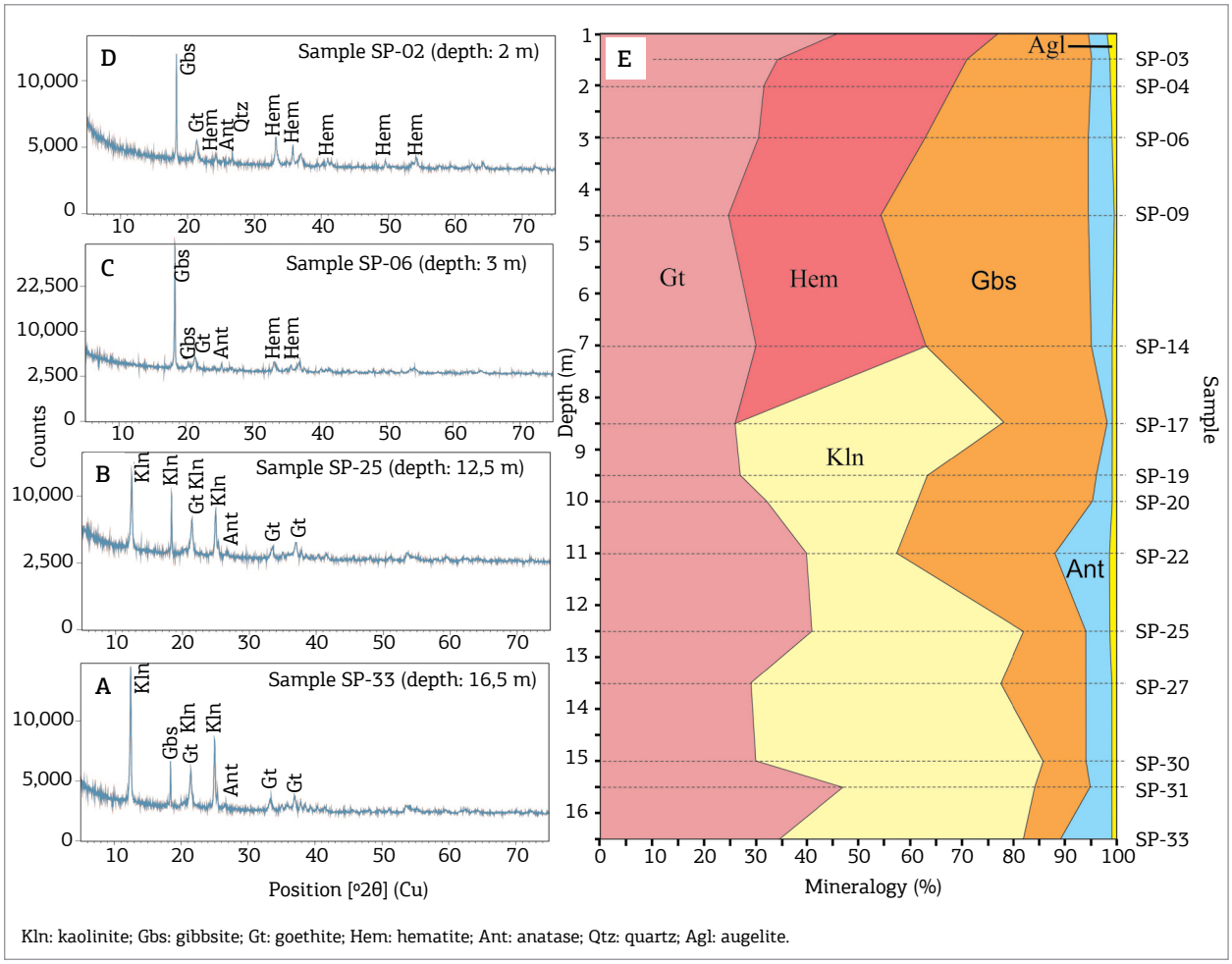

Kln: kaolinite; Gbs: gibbsite; Gt: goethite; Hem: hematite; Ant: anatase; Qtz: quartz; Agl: augelite.

Figure 3. X-ray diffraction mineral composition of the Piriá deposit. (A and B) bauxitic clay horizon; (C and D) aluminous iron crust; (E) vertical distribution of the minerals that comprise the lateritic profile between 1.0 and 16.5 m deep (weight %).

Aluminous iron crust

The aluminous iron crust is compact and ferruginous nodules (Fig. 7A) and pisolites (Figs. 7B and 7C) are common. These materials are cemented by a brown micro to cryptocrystalline plasm. The crust is cavernous and the cavities are generally coated by dark brown microcrystalline film.

The aluminous iron comprises concretions (Fig. 7D), nodules (Fig. 7E) and even oolites and pisolites (Fig. 7F), evolved by a microfractured plasm. The oolitic and pisolitic parts are represented by iron alterorelicts with concentric hematite layers, cemented by microcrystalline gibbsite. Some of these oolites and pisolites have relict quartz nuclear

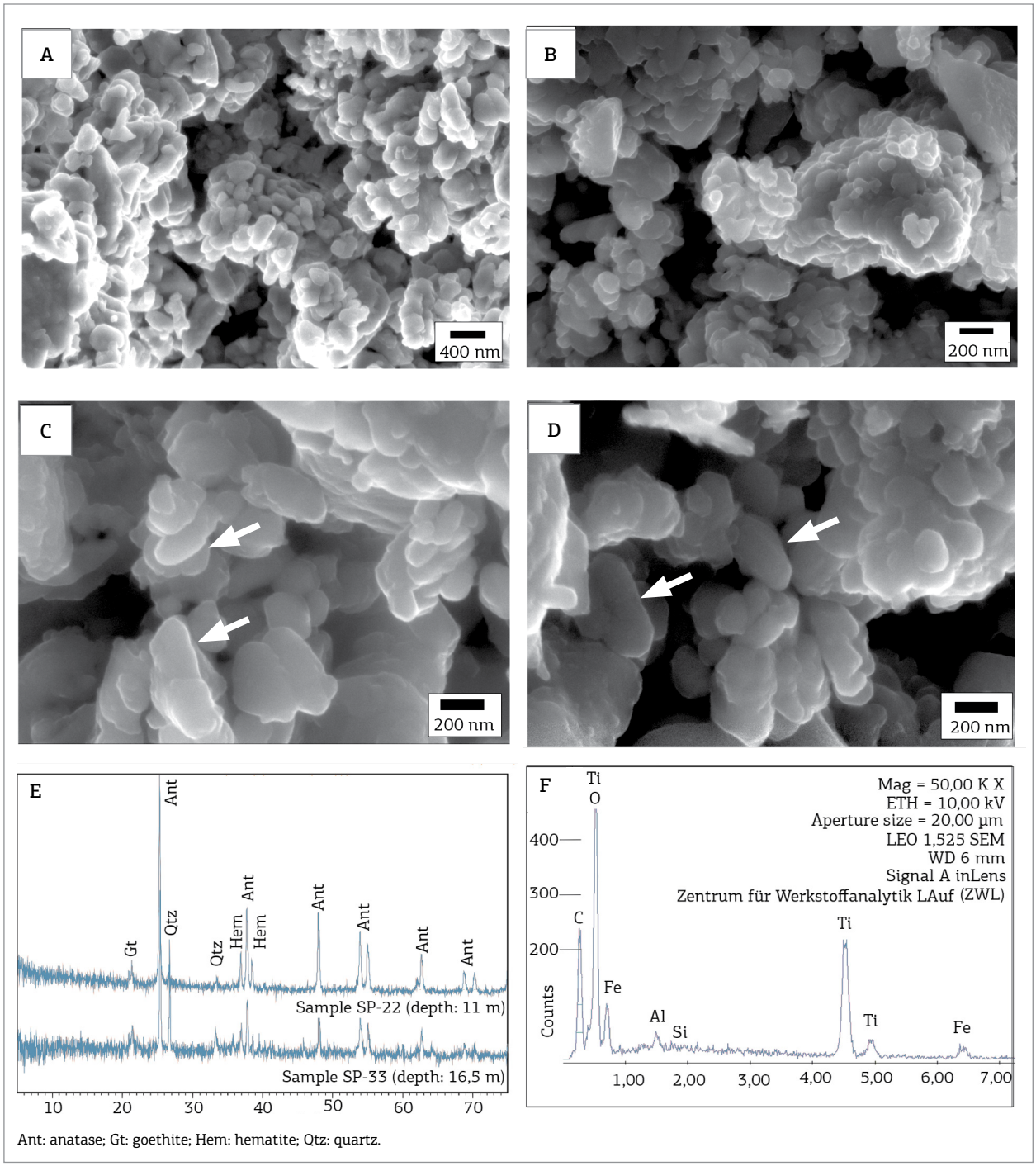

Figure 4. (A-D) anatase crystal morphologies with arrows indicating bipyramidal prismatic crystallites; (E) X-ray diffractograms of the concentrates obtained after the acidic treatment of the bauxitic clay samples showing that the anatase domain contains relict goethite, hematite and quartz; (F) anatase chemical spectrum obtained by scanning electron microscopy/energy dispersive spectrometry.

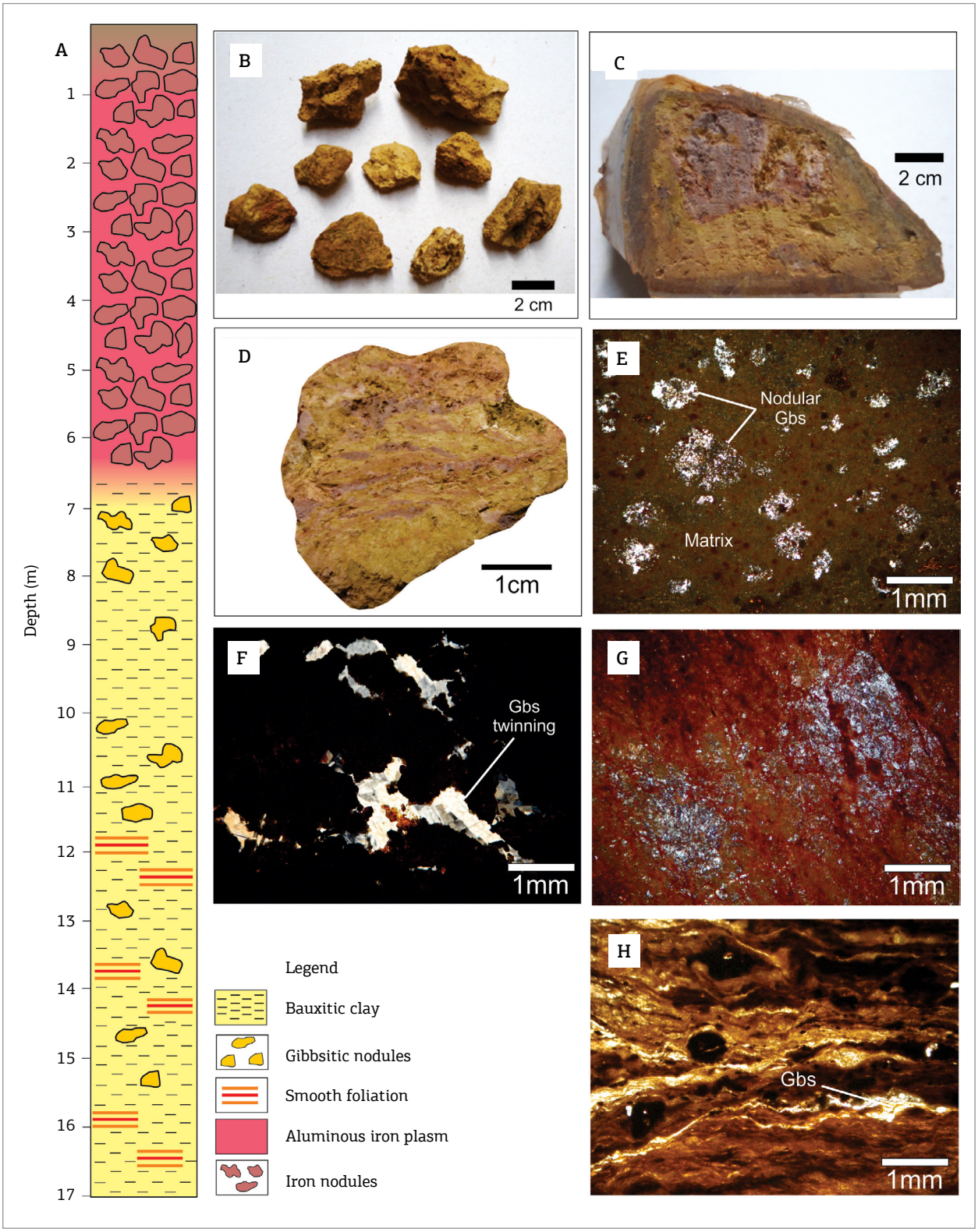

Figure 5. (A) The Piriá ridge lateritic profile, divided into a bauxitic clay horizon (7 to 17 m deep) and aluminous iron crust (above 7 m deep). Bauxitic clay horizon; (B) gibbsite nodules; (C) mottled bauxitic clay; (D) smooth foliated bauxitic clay fragment; (E) microcrystalline gibbsite nodules in kaolinite + goethite matrix, under cross-polarized light; (F) mesocrystalline gibbsite with albite type twinning that developed in microcavities, under cross-polarized light; (G) clay matrix that is associated with gibbsite crystallites and spotted by goethite, under cross-polarized light; (H) smooth foliation that comprises yellowish, brownish and subtranslucent bands, under parallel-polarized light.

germs. Microcrystalline gibbsite fills the cavities and fractures of this horizon, and the cement is composed of gibbsitic crystalliplasma with hematite + goethite impregnation, similar to the bauxitic clay horizon.

Locally, the crust exhibits reliquiar quartz grains associated with the ferruginous nodules and cemented by the aluminous iron plasm (Fig. 7G). The grains display gulf-type irregular edges, suggesting corrosion.

Geochemistry and mineralogy

The bulk rock chemical composition shows SiO_2, Al_2O_3 and Fe_2O_3 domains (Tab. 1), which confirms the mineral data

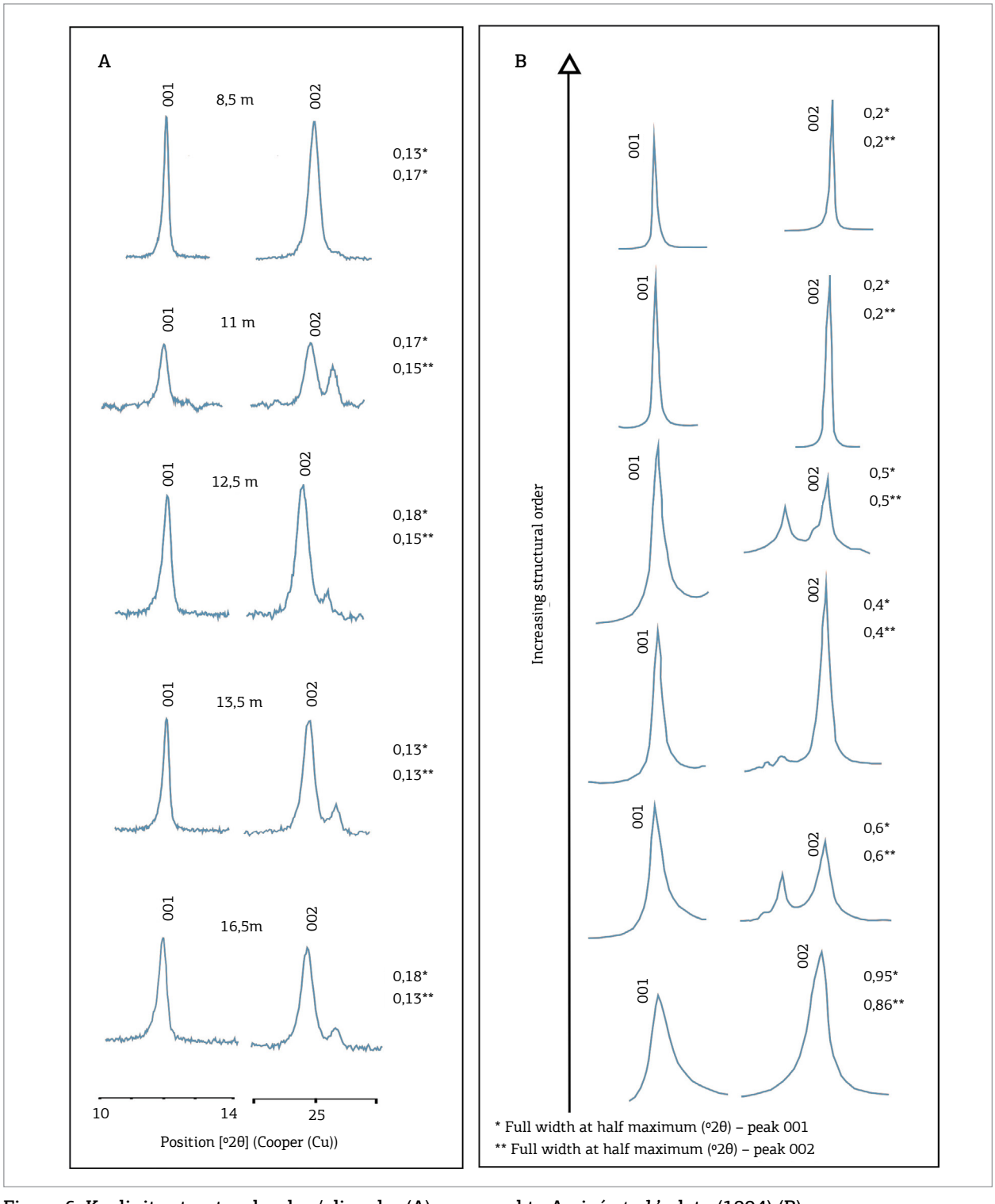

Figure 6. Kaolinite structural order / disorder (A) compared to Amigó *et al.*'s data (1994) (B).

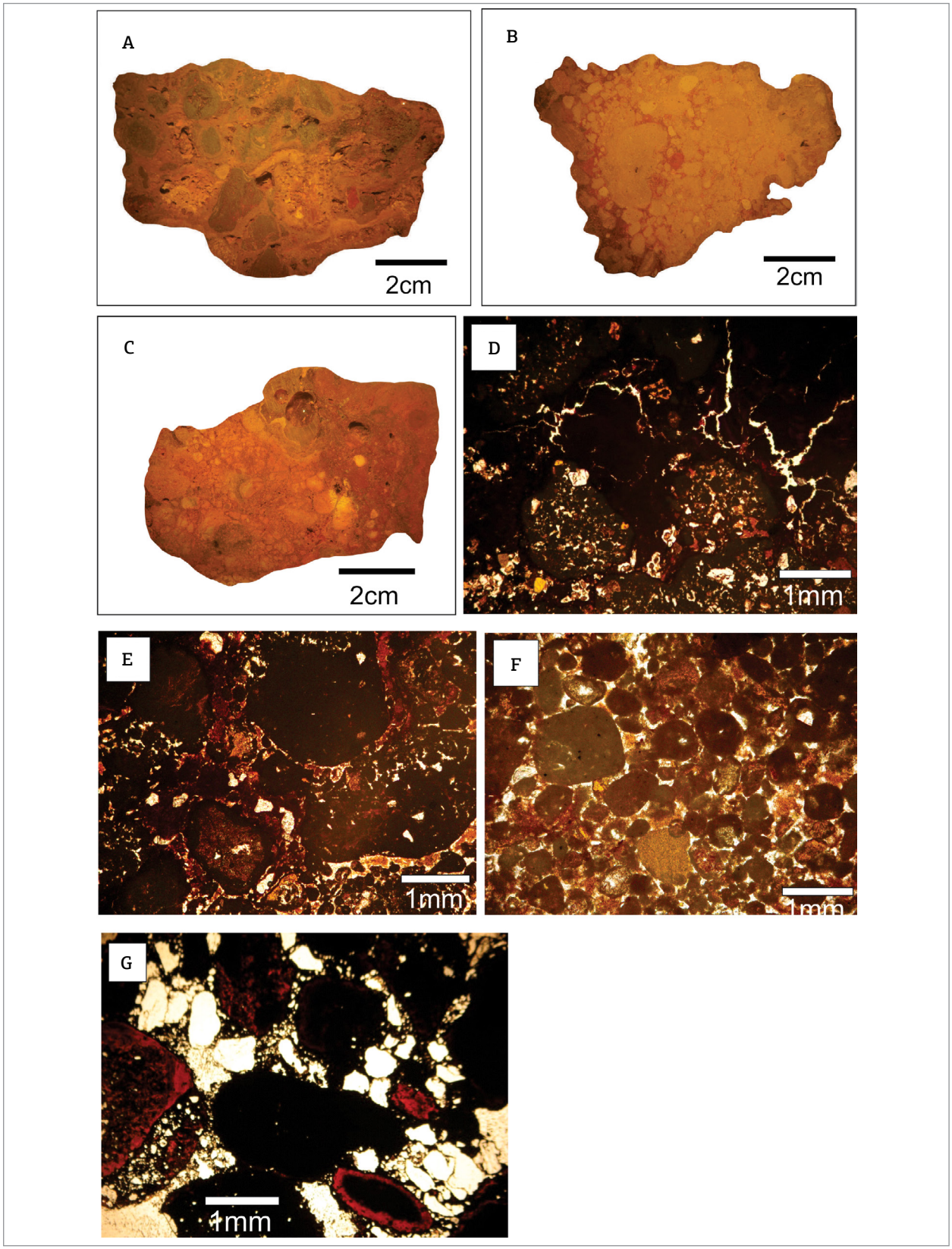

Figure 7. Aluminous iron crust meso and micromorphology. (A) Ferruginous nodules cemented by aluminous iron plasm; (B) pisolites cemented by aluminous iron plasm; (C) pisolitic crust in contact with nodular bauxite; (D) iron concretions within microfractured plasm; (E) iron nodules and oolites that are cemented by goethitic-hematitic-gibbsitic plasm; (F) pisolitic iron features in gibbsitic crystalliplasma; (G) nodular crust that comprises iron oxy-hydroxides and quartz grains.

Table 1. Chemical composition expressed in weight % (for major elements) and ppm (for trace elements).

Sample	SP-01	SP-02	SP-03	SP-04	SP-05	SP-06	SP-07	SP-08	SP-09	SP-10	SP-13	SP-14	SP-15	SP-16	SP-17	SP-18	SP-19
Depth (m)	0.5	1.0	1.5	2.0	2.5	3.0	3.5	4.0	4.5	5.0	6.5	7.0	7.5	8.0	8.5	9.0	9.0
SiO_2	11.70	4.85	1.22	0.84	0.50	0.52	0.56	0.50	0.48	0.55	0.89	0.98	13.20	28.20	24.50	24.80	16.50
Al_2O_3	8.53	11.80	16.30	21.10	25.90	28.70	27.10	24.10	22.50	23.80	23.70	21.00	35.40	36.60	34.30	35.30	35.40
Fe_2O_3	67.8	69.3	67.4	59.4	52.4	47.4	50.3	55.8	57.2	55.1	55.0	60.0	28.7	15.6	21.7	21.5	26.0
CaO	0.03	0.02	0.01	0.03	0.02	<0.01	0.03	0.01	0.02	0.01	0.02	0.03	0.01	<0.01	<0.01	0.02	<0.01
TiO_2	2.99	3.35	3.59	4.12	4.88	4.70	4.80	4.28	5.70	5.50	5.29	4.21	3.11	1.15	1.14	1.62	2.66
P_2O_5	0.718	0.649	0.518	0.405	0.514	0.486	0.543	0.447	0.206	0.244	0.372	0.301	0.357	0.162	0.224	0.258	0.331
MnO	0.03	0.04	0.04	0.05	0.06	0.07	0.05	0.03	0.04	0.03	0.06	0.04	0.01	<0.01	<0.01	<0.01	0.01
LOI	8.46	10.40	11.86	14.19	15.93	18.09	17.32	15.56	14.35	14.73	15.36	14.01	19.05	17.19	17.06	17.39	18.80
Total	100.3	100.4	100.9	100.1	100.2	100.0	100.7	100.7	100.5	100.0	100.7	100.6	99.8	98.9	98.9	100.9	99.7
Ag	na	0.9	na	0.3	na	0.3	na	na	0.5	na	na	5.6	na	na	0.1	na	na
As	na	13.8	na	10.4	na	9.5	na	na	10.4	na	na	7.1	na	na	4.9	na	na
Ba	na	4	na	2	na	3	na	na	3	na	na	2	na	na	5	na	na
Co	na	6.0	na	7.3	na	13.1	na	na	6.0	na	na	15.8	na	na	5.3	na	na
Cr	na	104.0	na	102.0	na	98.0	na	na	100.0	na	na	82.0	na	na	74.0	na	na
Cu	na	80.3	na	104.7	na	142.8	na	na	45.7	na	na	83.5	na	na	43.2	na	na
Ga	na	47.2	na	39.2	na	48.2	na	na	50.0	na	na	44.2	na	na	26.7	na	na
Hf	na	6.5	na	8.8	na	8.7	na	na	9.9	na	na	9.3	na	na	5.1	na	na
Hg	na	0.31	na	0.52	na	0.22	na	na	0.16	na	na	0.32	na	na	0.11	na	na
Mo	na	1.8	na	1.5	na	1.8	na	na	1.6	na	na	1.5	na	na	0.9	na	na
Nb	na	16.1	na	21.4	na	22.7	na	na	26.9	na	na	23.5	na	na	7.0	na	na
Ni	na	10.3	na	17.7	na	49.3	na	na	24.7	na	na	53.5	na	na	16.3	na	na
Pb	na	6.1	na	3.5	na	6.3	na	na	4.6	na	na	4.7	na	na	0.9	na	na
Sb	na	1.4	na	1.4	na	2.6	na	na	2.1	na	na	2.0	na	na	0.6	na	na
Sc	na	53	na	50	na	70	na	na	50	na	na	57	na	na	32	na	na
Sn	na	3	na	3	na	3	na	na	4	na	na	4	na	na	1	na	na
Sr	na	7.8	na	5.1	na	6.3	na	na	4.1	na	na	6.7	na	na	5.0	na	na
Ta	na	1.1	na	1.4	na	1.4	na	na	1.6	na	na	1.6	na	na	0.6	na	na
Th	na	5.6	na	5.2	na	6.3	na	na	4.3	na	na	4.9	na	na	5.2	na	na
U	na	0.7	na	0.9	na	1.1	na	na	0.7	na	na	1.0	na	na	1.6	na	na
V	na	1179	na	1188	na	999	na	na	1327	na	na	1079	na	na	691	na	na
W	na	1.7	na	1.7	na	1.9	na	na	2.0	na	na	2.3	na	na	0.7	na	na
Y	na	5.9	na	6.5	na	8.8	na	na	7.1	na	na	10.0	na	na	6.2	na	na
Zn	na	44	na	45	na	98	na	na	42	na	na	107	na	na	59	na	na
Zr	na	258.2	na	324.5	na	336.7	na	na	380.6	na	na	351.8	na	na	174.8	na	na
La	na	6.3	na	5.2	na	6.8	na	na	5.1	na	na	7.7	na	na	14.0	na	na
Ce	na	11.8	na	9.0	na	16.7	na	na	9.4	na	na	13.2	na	na	10.9	na	na
Pr	na	1.29	na	1.16	na	1.67	na	na	0.92	na	na	1.58	na	na	1.52	na	na
Nd	na	4.6	na	4.4	na	6.9	na	na	3.3	na	na	6.2	na	na	4.9	na	na
Sm	na	1.11	na	0.84	na	1.64	na	na	0.76	na	na	1.55	na	na	0.88	na	na
Eu	na	0.30	na	0.33	na	0.56	na	na	0.27	na	na	0.50	na	na	0.33	na	na
LREE	-	25.40	-	20.93	-	34.27	-	-	19.75	-	-	30.73	-	-	32.53	-	-
Gd	na	0.99	na	1.05	na	1.67	na	na	0.87	na	na	1.70	na	na	1.10	na	na
Tb	na	0.20	na	0.20	na	0.32	na	na	0.19	na	na	0.30	na	na	0.20	na	na
Dy	na	1.36	na	1.45	na	2.02	na	na	1.17	na	na	1.94	na	na	1.38	na	na
Ho	na	0.26	na	0.34	na	0.42	na	na	0.30	na	na	0.45	na	na	0.26	na	na
Er	na	0.99	na	1.21	na	1.61	na	na	1.18	na	na	1.48	na	na	0.75	na	na
Tm	na	0.19	na	0.25	na	0.30	na	na	0.29	na	na	0.29	na	na	0.14	na	na
Yb	na	1.57	na	1.95	na	2.46	na	na	2.33	na	na	2.30	na	na	0.87	na	na
Lu	na	0.26	na	0.36	na	0.44	na	na	0.48	na	na	0.47	na	na	0.18	na	na
∑ HREE	-	5.81	-	6.81	-	9.24	-	-	6.81	-	-	8.93	-	-	4.88	-	-
∑ REE	-	31.22	-	27.74	-	43.51	-	-	26.56	-	-	39.66	-	-	37.41	-	-
LREE/HREE	-	4.36	-	3.07	-	3.71	-	-	2.90	-	-	3.44	-	-	6.67	-	-
(La/Lu)n	-	2.47	-	1.47	-	1.58	-	-	1.08	-	-	1.67	-	-	7.94	-	-

Continue...

Table 1. Continuation.

Sample	SP-20	SP-21	SP-22	SP-23	SP-24	SP-25	SP-26	SP-27	SP-28	SP-29	SP-30	SP-31	SP-32	SP-33	SP-34
Depth (m)	**10.0**	**10.5**	**11.0**	**11.5**	**12.0**	**12.5**	**13.0**	**13.5**	**14.0**	**14.5**	**15.0**	**15.5**	**16.0**	**16.5**	**17.0**
SiO_2	13.2	10.2	7.78	11.3	14.4	17.6	19.7	22.0	26.8	24.1	26.4	14.4	17.5	20.8	23.6
Al_2O_3	33.1	28.9	29.4	28.1	26.6	23.2	27.0	29.8	29.1	29.0	28.4	19.1	21.3	25.2	25.7
Fe_2O_3	30.7	38.4	39.4	38.6	38.9	42.2	33.0	26.2	25.5	27.7	26.9	49.2	44.7	36.0	32.9
CaO	<0.01	<0.01	0.02	0.01	0.01	0.01	0.01	0.02	0.01	0.01	0.01	0.02	<0.01	<0.01	<0.01
TiO_2	3.47	4.44	5.20	4.84	3.97	3.77	4.61	5.03	5.14	4.93	5.14	3.55	3.88	4.42	4.64
P_2O_5	0.358	0.428	0.487	0.493	0.409	0.397	0.363	0.326	0.328	0.379	0.371	0.298	0.243	0.279	0.221
MnO	0.01	0.03	0.04	0.05	0.05	0.06	0.06	0.03	0.05	0.06	0.05	0.08	0.06	0.07	0.08
LOI	18.53	17.44	18.04	17.15	15.79	13.33	14.67	15.28	14.07	14.67	14.00	11.93	12.20	13.35	12.89
Total	99.4	99.8	100.4	100.5	100.1	100.6	99.4	98.7	101.0	100.8	101.3	98.6	99.9	100.1	100.0
Ag	0.5	na	na	0.5	na	1.3	na	0.2	na	na	0.7	10.3	na	na	<0.1
As	4.6	na	na	2.0	na	4.5	na	2.1	na	na	4.4	12.3	na	na	7.0
Ba	4	na	na	5	na	2	na	3	na	na	6	2	na	na	<1
Co	14.3	na	na	23.2	na	20.0	na	14.0	na	na	12.5	14.1	na	na	15.0
Cr	79.0	na	na	95.0	na	87.0	na	60.0	na	na	47.0	32.0	na	na	0.0
Cu	83.2	na	na	129.7	na	116.8	na	109.3	na	na	134.1	123.5	na	na	141.8
Ga	33.6	na	na	47.9	na	33.9	na	42.2	na	na	41.1	34.0	na	na	33.6
Hf	7.0	na	na	10.2	na	7.4	na	9.4	na	na	9.9	7.8	na	na	7.7
Hg	0.07	na	na	0.10	na	0.06	na	0.09	na	na	0.04	0.04	na	na	0.03
Mo	0.8	na	na	0.7	na	0.4	na	0.5	na	na	0.6	0.4	na	na	1.2
Nb	16.3	na	na	23.7	na	18.4	na	23.4	na	na	22.6	19.7	na	na	19.9
Ni	48.0	na	na	77.5	na	54.0	na	55.4	na	na	46.3	42.8	na	na	56.3
Pb	1.5	na	na	3.6	na	5.1	na	2.1	na	na	2.6	4.8	na	na	3.7
Sb	1.0	na	na	1.3	na	0.7	na	0.8	na	na	0.7	0.6	na	na	0.5
Sc	61	na	na	95	na	82	na	91	na	na	110	81	na	na	68
Sn	3	na	na	4	na	4	na	4	na	na	4	3	na	na	3
Sr	8.2	na	na	14.2	na	5.3	na	10.7	na	na	16.9	5.5	na	na	0.7
Ta	1.1	na	na	1.7	na	1.1	na	1.5	na	na	1.4	1.3	na	na	1.2
Th	4.7	na	na	6.4	na	2.8	na	3.3	na	na	2.7	1.9	na	na	2.1
U	1.5	na	na	1.8	na	1.1	na	1.0	na	na	1.3	0.8	na	na	0.8
V	918	na	na	1272	na	888	na	665	na	na	686	771	na	na	547
W	1.1	na	na	2.4	na	1.6	na	1.6	na	na	2.0	1.9	na	na	2.8
Y	6.4	na	na	9.4	na	10.0	na	8.0	na	na	7.5	7.5	na	na	8.2
Zn	122	na	na	164	na	117	na	110	na	na	102	92	na	na	101
Zr	250.3	na	na	382.9	na	295.2	na	367.4	na	na	366.2	305.0	na	na	301.9
La	16.2	na	na	20.0	na	7.6	na	12.6	na	na	24.1	11.2	na	na	1.1
Ce	22.8	na	na	33.3	na	15.5	na	29.7	na	na	34.4	15.3	na	na	3.3
Pr	2.56	na	na	3.75	na	1.76	na	3.01	na	na	4.01	1.66	na	na	0.40
Nd	7.5	na	na	12.6	na	6.7	na	10.9	na	na	11.9	5.7	na	na	1.8
Sm	1.47	na	na	2.37	na	1.57	na	1.58	na	na	2.02	1.12	na	na	0.68
Eu	0.37	na	na	0.62	na	0.50	na	0.39	na	na	0.50	0.35	na	na	0.27
∑ LREE	50.90	-	-	72.64		33.63	-	58.18	-	-	76.93	35.33	-	-	7.55
Gd	1.21	na	na	1.74	na	1.69	na	1.12	na	na	1.43	1.10	na	na	0.85
Tb	0.22	na	na	0.32	na	0.30	na	0.19	na	na	0.23	0.20	na	na	0.19
Dy	1.41	na	na	1.90	na	2.13	na	1.21	na	na	1.26	1.36	na	na	1.33
Ho	0.29	na	na	0.45	na	0.46	na	0.34	na	na	0.30	0.27	na	na	0.32
Er	1.04	na	na	1.44	na	1.56	na	1.30	na	na	1.24	1.16	na	na	1.38
Tm	0.21	na	na	0.34	na	0.29	na	0.31	na	na	0.27	0.24	na	na	0.26
Yb	1.61	na	na	2.67	na	2.38	na	2.50	na	na	2.34	2.13	na	na	2.19
Lu	0.33	na	na	0.50	na	0.43	na	0.47	na	na	0.45	0.43	na	na	0.40
∑ HREE	6.32	-	-	9.36	-	6.86	-	4.94	-	-	7.52	6.89	-	-	6.92
∑ REE	51.23	-	-	73.14	-	34.06	-	58.65	-	-	77.38	35.76	-	-	7.95
LREE/ HREE	8.05	-	-	7.76	-	4.90	-	11.78	-	-	10.23	5.13	-	-	1.09
(La/Lu)n	5.01	-	-	4.08	-	1.80	-	2.74	-	-	5.46	2.66	-	-	0.28

na: not analyzed.

(kaolinite, gibbsite and hematite + goethite). The silica content ranges from 0.48 to 26.78%, decreasing from the base towards the top of the profile, with an anomalous increase at the superficial part of the profile, which corresponds to the transition from the iron aluminous crust to the covering soil (Fig. 8). These contents reflect the variable kaolinite content, which is abundant at the base and absent near the top of the profile. The Fe_2O_3 content displays an inverse behavior compared to SiO_2, which is typical of lateritic profiles, and ranges from 15.6 to 69.3%, which is higher than in the aluminous iron crust.

The Al_2O_3 content ranges from 8.53 to 36.00% and increases upward over the bauxitic clay horizon, similarly to LOI, but decreases upward over the aluminous iron crust, and oscillates positively between 2.5 and 4.0 m because of weak gibbsite enrichment (Fig. 8). Both Al_2O_3 and LOI are associated with gibbsite, kaolinite and Al-goethite abundance. TiO_2 and P_2O_5 contents are higher than the crustal average, ranging from 0.65 to 5.70% and 0.16 to 0.72%, respectively, and represented only by anatase and augelite. LOI ranges from 8.46 to 19.05%, housed in the structure of kaolinite, goethite and mainly gibbsite. The transition from bauxitic clay to aluminous iron crust is sharp in terms of SiO_2, Al_2O_3 and Fe_2O_3 content.

The analyzed trace elements Ag, Ba, Co, Cr, Mo, Ni, Pb, Sn, Sr, Th, U, Y, and REE (except Lu) are below the crustal average throughout all the profile. On the other hand, As, Cu, Ga, Hf, Nb, Sb, Sc, V, Zn and Zr exhibit values above the crustal average, especially As, Cu, Sb, Sc and V (Tab. 1). The contents of these elements increase upwards, similarly

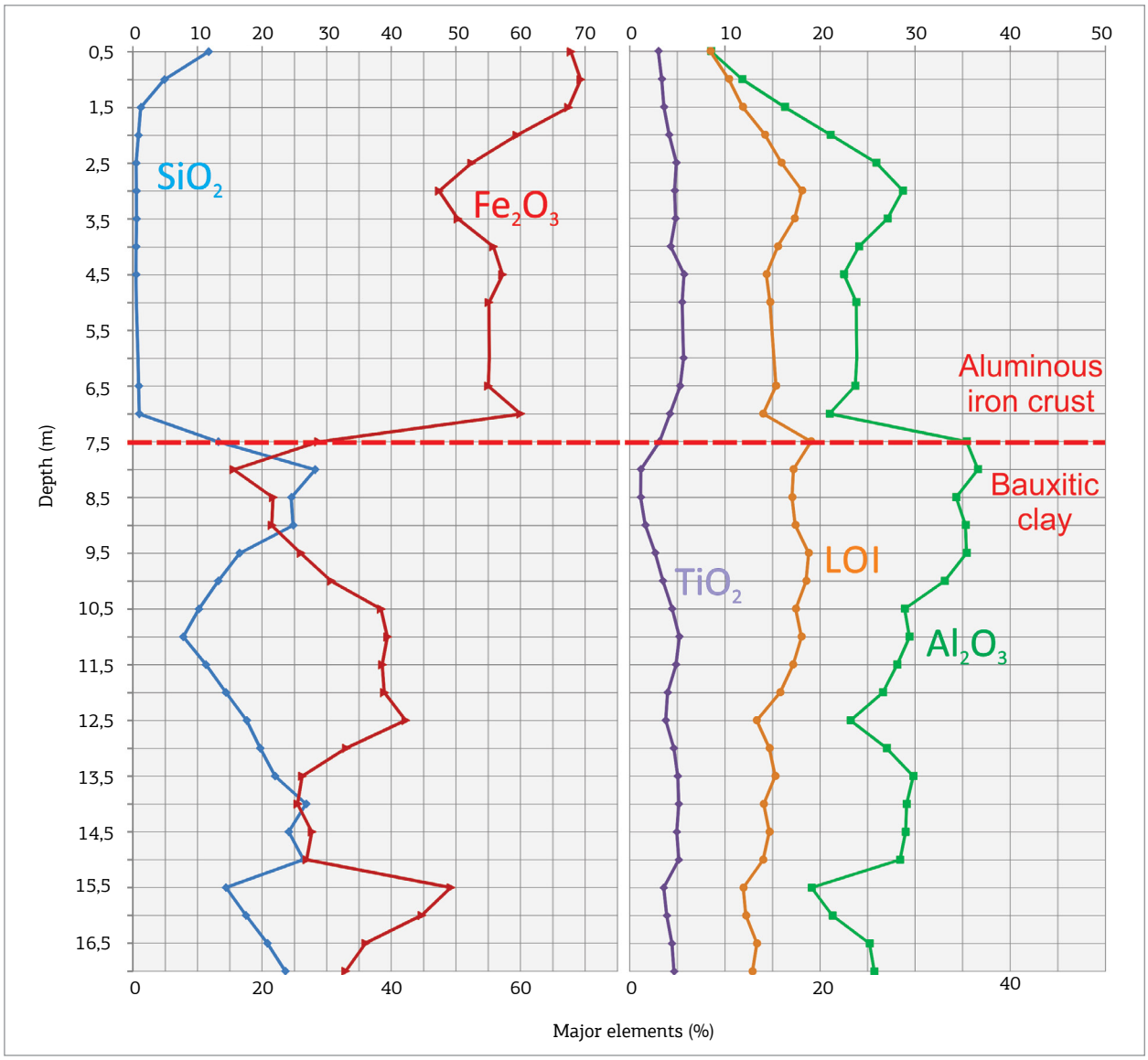

Figure 8. Distribution of major element contents throughout the Piriá Ridge lateritic profile. (A) SiO_2 and Fe_2O_3. (B) TiO_2, Al_2O_3 and Lost of Ignition.

to the iron contents, with whom they have a strong positive relationship, in the form of oxy-hydroxides.

The significant negative correlations of Fe_2O_3 × SiO_2 and Fe_2O_3 × Al_2O_3 highlight the lateritic evolution and the distinct domains of the bauxitic clay horizon and bauxitic ferruginous crust in the studied profile. The LOI exhibits virtually similar behavior to Al_2O_3, and both have more elevated values from 14.0 to 17.5 m depth, which clearly delimits a more bauxitic zone. Thus, the Piriá ridge lateritic profile is equivalent to the complete and mature lateritic profiles from Costa (1991), which did not complete their transformation of kaolinite to gibbsite.

The Fe_2O_3 × TiO_2 and Al_2O_3 × TiO_2 correlations suggest two chemical domains, which are indicated by both positive and negative correlations among them (Figs. 9A and 9B), because Ti and Al are low-mobility elements, the opposite of iron, which has high mobility. This observation infers that the parent rock had distinct Ti and Al compositions. One domain was more felsic (poor in TiO_2) and another was more mafic (rich in TiO_2 compared to Al_2O_3). The strong variations in TiO_2 content reflect the chemical heterogeneity of this parent rock. Fe_2O_3 well correlates with V and As (Figs. 9C and 9D).

A strongly positive Zr × Hf correlation (Fig. 10A), with a nearly constant correlation coefficient of 0.98, indicates only one source of zircon, which is the only mineral that holds these elements in the investigated profile. Moreover, the Zr/Hf ratio of 38 fits the zircon variation interval (Barros *et al.* 2005). The Nb × Ta correlation is also very significant (Fig. 10B) and zircon is known to contain low amounts of Nb and Ta because these elements correlate positively to Zr and Hf (Figs. 10C and 10D), and an Nb/Ta ratio of 15.25 is commonly observed in zircon (Barros *et al.* 2005).

The positive correlation between Zr and Heavy Rare Earth Elements (HREE) indicates that zircon is the main REE holder (Figs. 10E–10G). On the other hand, TiO_2 presents positive correlation with HREE (Figs. 10H-10J), the same elements that correlates to Zr, suggesting that anatase accumulated similarly to zircon throughout the lateritic profile, although the first is newly formed and the second is resistate.

In the SiO_2 × Al_2O_3 × Fe_2O_3 ternary diagram (Fig.11), both horizons are even clearer, and the so-called bauxitic clay horizon, according to the Bardossy (1982) classification, comprises clay bauxite, bauxitic clay, ferruginous bauxite and bauxite that are poor in iron, while the bauxitic ferruginous crust is totally equivalent to this classification. According to Aleva and Creutzberg's (1994) classification, the so-called bauxitic clay horizon only comprises laterites and the bauxitic ferruginous crust mainly comprises bauxitic ferrite. The broad domain of Fe_2O_3 throughout the lateritic profile also suggests iron-rich parent rock.

The REE are virtually under the crustal average, and their contents are similar to those in the majority of bauxitic

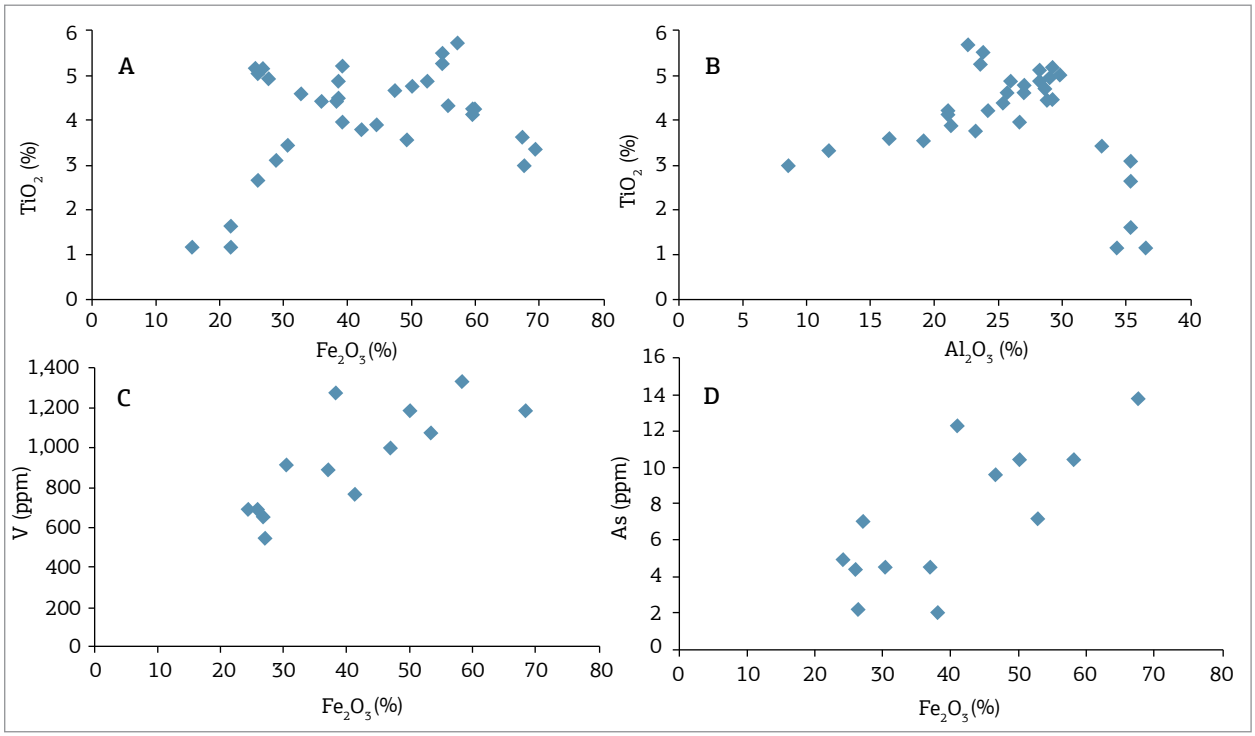

Figure 9. Geochemical correlations along the Piriá ridge lateritic profile. (A) Fe_2O_3 × TiO_2; (B) Al_2O_3 × TiO_2; (C) Fe_2O_3 × V; (D) Fe_2O_3 × As.

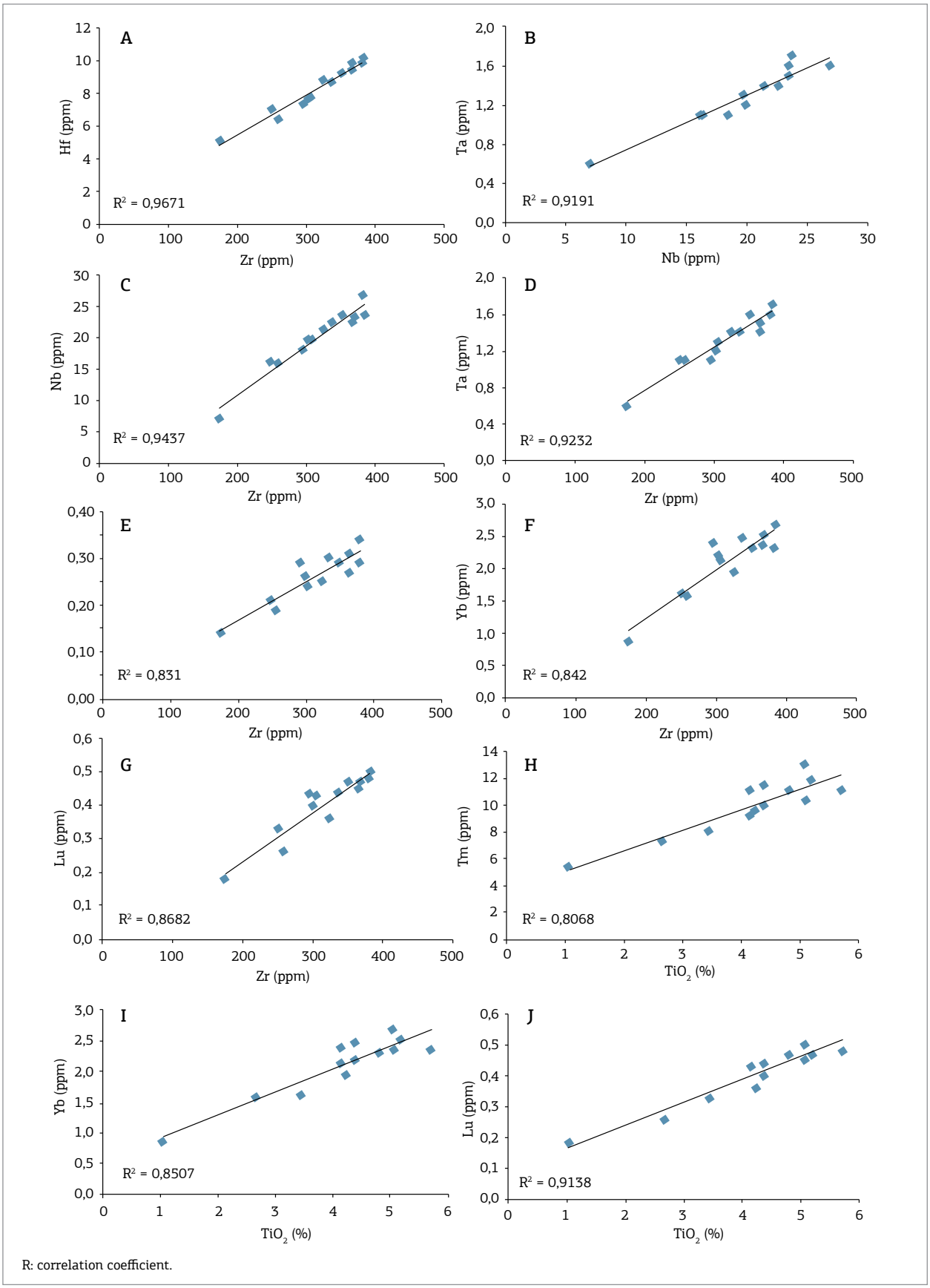

R: correlation coefficient.

Figure 10. Geochemical correlations along Piriá ridge lateritic profile. (A) Zr × Hf; (B) Nb × Ta; (C) Zr × Nb; (D) Zr × Ta; (E) Zr × Tm; (F) Zr × Yb; (G) Zr × Lu; (H) TiO_2 × Tm; (I) TiO_2 × Yb; (J) TiO_2 × Lu.

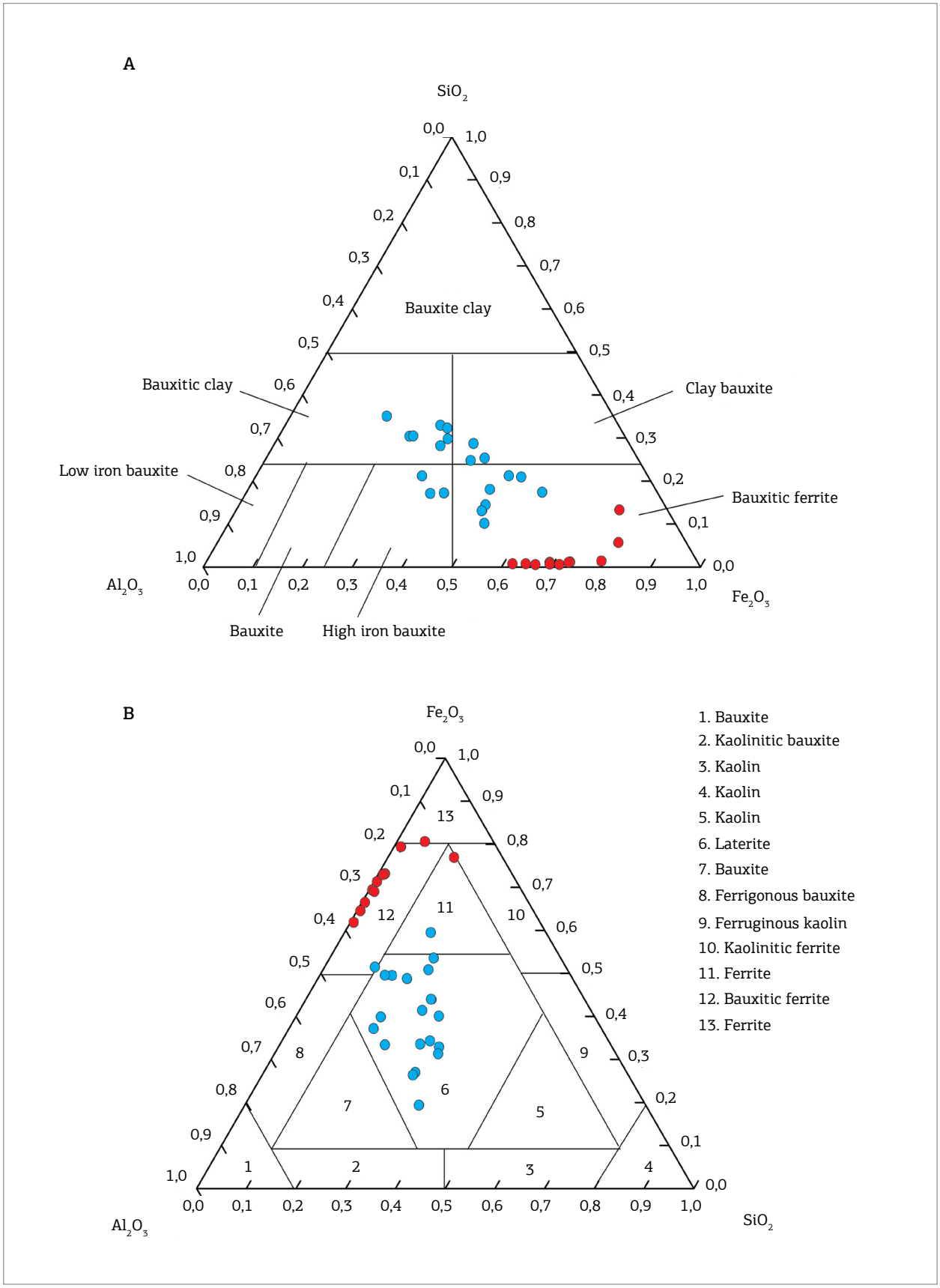

Figure 11. Chemical classification of the bauxitic clay horizon (blue circles) and the bauxitic ferruginous crust (red circles). (A) on the Bardossy (1982) diagram; (B) on the Aleva & Creutzberg (1994) diagram.

lateritic profiles that originated from sedimentary rocks (Horbe & Costa 1999, Kotschoubey *et al.* 2005) and granitoids (Du *et al.* 2012, Giorgis *et al.* 2014). These elements are more abundant in the bauxitic clay, with the sum of Rare Earth Elements (ΣREE) of 53.3 ppm, while the ΣREE in the bauxitic ferruginous crust is 33.7 ppm. The REE distribution patterns, when normalized by chondrites, are similar in both horizons. However, positive Ce and negative Eu anomalies were not observed, which is uncommon in lateritic profiles (Horbe & Costa 1997, Horbe & Costa 1999, Du *et al.* 2012, Giorgis *et al.* 2014).

The curves show "open U" forms (Fig. 12) with light enrichment in light REE compared to heavy REE, as indicated by $(La/Lu)_n$ (Tab. 1), which is similar to the pattern that was observed by Kotschoubey *et al.* (2005) in different horizons from the Paragominas bauxitic province (saprolite, bauxite, ferruginous horizon and clay cover) and developed over siliciclastic rocks. A significant positive correlation among the REE, TiO_2 and Zr contents was also observed, which suggests that these elements were contained within zircon structure or maybe anatase, as proposed by Barros *et al.* (2005).

DISCUSSIONS

The horizontal geometry of the succession, the distinct geomorphological configuration of the occurrence at the terrane and the pattern of the mineral distribution in the Piriá deposit profile are similar to the majority of the mature and complete lateritic profiles that are associated with bauxite in the Amazon region (Dennen & Norton 1977, Costa 1980, Costa 1991, Calaf 2000, Horbe & Costa 1999, Kotschoubey *et al.* 2005, Costa *et al.* 2014), thereby this deposit can be interpreted as being formed during the same lateritization event at the Paleocene time. The studied drill cores did not reach fresh rocks, so the parent rocks of the deposit were not examined or discussed. The iron and clay (kaolinite) rich profile has economic interest with potential for supply of raw material for the cement industry, and was used for this purpose some years ago. The iron minerals are represented by hematite, goethite and also Al-goethite, imprinting the red to yellowish color of the whole investigated profile.

Observations, from the base to the top of the profile, indicate a continuous process of dissolution of kaolinite, and formation of gibbsite, so that the aluminum content in ferroaluminous crust is higher than in the bauxitic clay. Similarly, a continuous process of hematite formation from goethite resulting from the modification to more arid climate conditions is interpreted. This process of crust generation advanced from the top to the base of the profile up to 7 m depth. Above this depth, no kaolinite was identified by XRD, and below that no hematite was detected.

When the average chemical compositions are compared to other lateritic profiles (Tab. 2), originated from granites, Balkouin in Burkina Faso (Giorgis *et al.* 2014); ultramafic rock, Barro Alto, in Brazil (Oliveira *et al.* 2013); and carbonate rock, Guangxi, in China (Liu *et al.* 2012), it showed more similarity to Barro Alto deposit, which is derived from anorthosites. This relation to mafic rocks is also indicated by

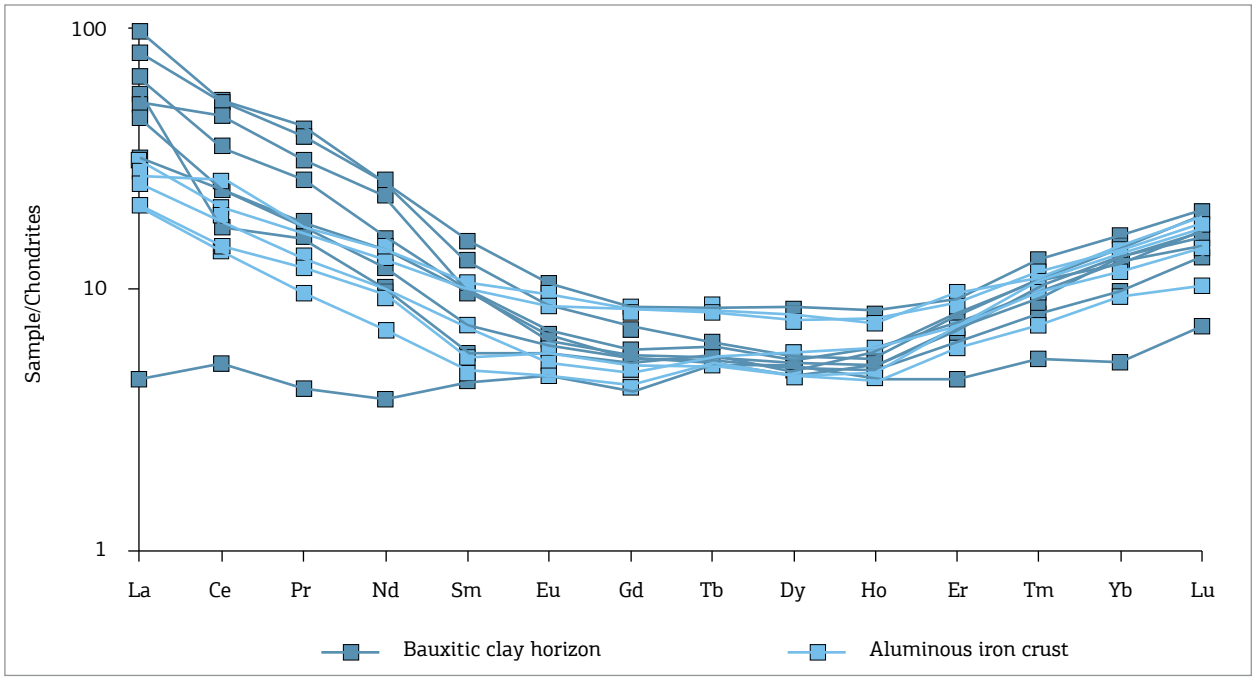

Figure 12. Rare Earth Elements distribution patterns, normalized by Evensen et al. (1978) chondrites.

Table 2. Chemical comparison between Piriá ridge and some lateritic profiles and carstic bauxite around the world.

Element	Piriá ridge average	Crustal average (Widepohl 1995)	Granitic origin (Giorgis *et al.* 2014)	Ultramafic origin (Oliveira *et al.* 2013)	Carstic bauxite (Liu *et al.* 2012)
SiO_2 (%)	12.52	61.50	19.05	22.62	6.73
Al_2O_3	26.11	15.10	16.25	49.74	43.70
Fe_2O_3	41.90	6.28	54.90	2.73	32.94
CaO	0.02	5.50	0.11	0.01	0.14
TiO_2	4.07	0.77	0.51	0.38	4016
P_2O_5	0.38	0.18	0.21	0.02	0.04
MnO	0.05	0.10	0.02	na	0.03
LOI	15.10	-	9.77	na	11.26
Ag (ppm)	1.77	0.07	na	na	na
As	7.15	1.70	na	na	7.61
Ba	3.42	584.00	18.80	na	18.00
Co	12.82	24.00	na	na	451.00
Cr	73.85	126.00	na	na	26.40
Cu	102.97	25.00	na	na	93.50
Ga	40.14	15.00	na	na	70.70
Hf	8.28	4.80	5.60	na	na
Hg	0.16	0.05	na	na	4.30
Mo	1.05	1.10	na	na	230.00
Nb	20.12	19.00	7.60	na	70.30
Ni	42.47	56.00	19.00	na	132.00
Pb	3.81	0.80	na	na	na
Sb	1.21	0.30	na	na	56.20
Sc	69.23	16.00	na	na	na
Sn	3.31	2.30	na	na	11.10
Sr	7.42	333.00	15.50	na	14.80
Ta	1.31	1.10	na	na	77.80
Th	4.26	8.50	19.85	na	17.30
U	1.10	1.70	3.43	na	232.00
V	939.23	98.00	na	na	na
W	1.82	1.00	na	na	71.40
Y	7.81	24.00	4.60	na	103.00
Zn	92.54	65.00	na	na	2274.00
Zr	315.04	203.00	200.00	na	na
La	10.61	30.00	12.90	na	na
Ce	17.33	60.00	26.40	na	na
Pr	1.95	6.70	3.22	na	na
Nd	6.72	27.00	11.00	na	na
Sm	1.35	5.30	2.08	na	na
Eu	0.41	1.30	0.55	na	na
Gd	1.27	4.00	1.44	na	na
Tb	0.24	0.65	0.22	na	na
Dy	1.53	3.80	1.15	na	na
Ho	0.34	0.80	0.22	na	na
Er	1.26	2.10	0.60	na	na
Tm	0.26	0.30	0.09	na	na
Yb	2.10	2.00	0.69	na	na
Lu	0.40	0.35	0.10	na	na

na: not analyzed.

the high TiO_2 and Fe_2O_3 in comparison to the low Al_2O_3 content, which is verified in almost the entire profile. This fact is confirmed by the Hallberg (1984) diagram (Fig. 13), except between depths of 9.5 and 7.5 m (from samples SP-19 to SP-15), in which the composition suggests granitoid parent rock (low TiO_2, low Fe_2O_3 and high Al_2O_3).

Anatase is a neoformed mineral, in changing quantity. There was observed a tendency of gradual increase in TiO_2 content upwards along the profile, as would be expected in most of the lateritic profiles. The high contents, however, oscillating, may be an indicative of compositional heterogeneity of bedrock along the profile, and also support a mafic composition.

Likely Al-goethite and kaolinite, anatase, in lateritic profiles, occurs in very small size (100 to 400 nm crystallites) and was identified by XRD. Under SEM, the anatase crystals present bipyramidal prismatic forms.

Iron released from decomposed primary minerals led to the formation of goethite which is prevalent aluminous (9.85 to 22.25%), which confers ocher color to the bauxitic clay horizon.

Considering the zircon stability, the REE shown distribution pattern is characteristic not of lateritic evolution, but of zircon geochemistry, a resistate mineral in the lateritic profile, which is confirmed by the absence of positive Ce anomaly (which may be oxidized to Ce^{4+} in laterite environment, forming cerianite). The high significant positive correlation REE × TiO_2 also may support an affinity between REE and anatase geochemistry, but zircon structure is more likely to hold REE than anatase and both zircon and anatase may have accumulated similarly along the profile, causing the high correlation of TiO_2 with the same elements hold by zircon.

Determination of the kaolinite's structural order by the XRD powder method was limited by the polymineralic nature of the samples, in which the kaolinite reflections are mainly overlapped by goethite reflections. Aparicio and Galán (1999) compared different methods to determine the kaolinite order/disorder grade: the Hinckley Index (HI); the Stoch Index (IK); the Range & Weiss Index (QF); the Lietard Index (R2); the Rughes & Brown Index (H & B); the Plaçon & Zacharie System; and FWHM 001/FWHM 002, which was proposed by Amigó *et al.* (1994). Among the investigated methods, only the last one (Amigó et al. 1994) is applicable to Piriá samples because the analyzed reflections, 001 and 002, are not overlapped by peaks from other minerals.

Using the Thiel (1963) method to calculate the aluminum content in goethite it was noted that aluminum, as in the majority of laterites, does not occur only in gibbsite, kaolinite or in aluminum phosphates structures, but it is also part of goethite, in which it replaces iron. Fe-Al substitution intensity is larger in the aluminous iron crust goethites than in the bauxitic clay goethites (Tab. 3), as result of the more intense dissolution of kaolinite in this horizon. After kaolinite dissolution (or even gibbsite dissolution) on Piriá ridge, aluminum replaced iron in all over the studied profile, ranging from 9.85 to 22.25 AlOOH moles %, with the maximum possible substitution being 33% according to Fitzpatrick and Schwertmann (1982).

CONCLUSIONS

The lateritic profile from Serra do Piriá can be well correlated to whose from Amazon region, mainly from Gurupi region, being similar to mature laterite profile. At least two typical horizons have been identified: a bauxitic clay horizon and a bauxitic ferruginous crust. The presence of bauxite and the absence of transitional compositions among the horizons, especially in terms of the Si and Fe contents, showed its structuration in well-individualized zones, which is typical of the Amazon's oldest mature lateritic profiles.

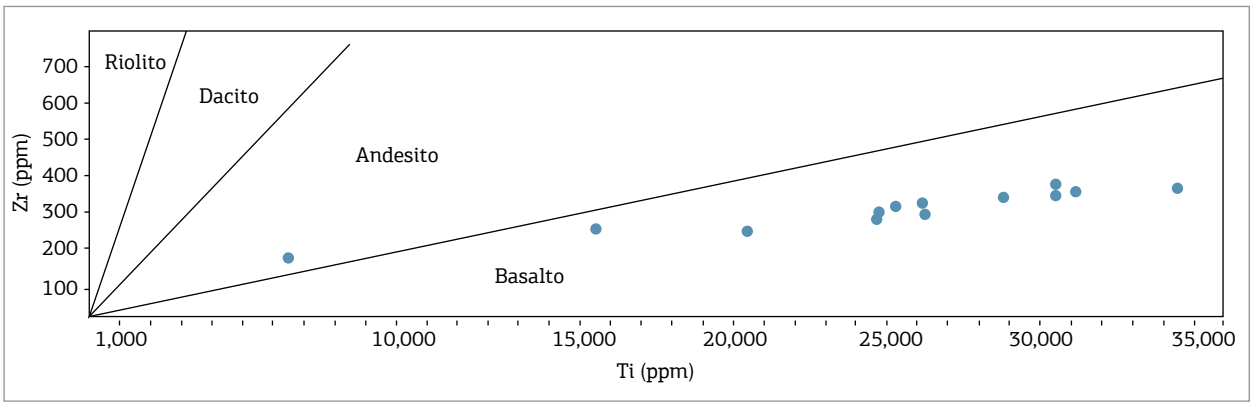

Figure 13. Ti and Zr contents plotted in the Hallberg (1984) diagram to differentiate the general nature of the parent rocks.

Table 3. AlOOH molar % in goethites, obtained from its respective reflections.

Horizon	Sample	Depth (m)	Positions of the main peaks				
			d_{140}	d_{111}	d_{121}	d_{130}	Average
Bauxitic ferruginous crust	SP-02	1.0	nd	13.99	nd	nd	13.99
	SP-03	1.5	nd	18.64	nd	nd	18.64
	SP-04	2.0	nd	22.25	nd	nd	22.25
	SP-06	3.0	24.24	23.19	11.74	nd	19.72
	SP-09	4.5	nd	23.5	nd	1.20	12.35
	SP-12	6.0	nd	19.46	nd	0.24	9.75
	SP-14	7.0	nd	16.85	nd	nd	16.85
Bauxitic clay	SP-17	8.5	11.58	10.81	12.81	13.21	12.10
	SP-19	9.5	12.58	13.51	11.65	13.28	12.75
	SP-20	10.0	15.78	13.96	13.64	14.40	14.45
	SP-22	11.0	11.89	14.90	12.95	15.97	13.93
	SP-25	22.5	14.31	14.99	11.75	17.19	14.56
	SP-27	13.5	13.58	14.21	10.68	15.10	13.39
	SP-30	15.0	12.33	14.21	14.30	15.36	14.05
	SP-31	15.5	12.96	11.21	12.89	nd	12.35
	SP-33	16.5	12.00	13.15	15.48	7.47	12.03

nd: not detected.

Although the bedrock was not investigated, the oscillating high contents of TiO_2 suggest mafic and heterogeneous parent rock respectively and some slightly foliation was still observed on bauxitic clay. This rock has undergone intensive lateritic weathering, probably during Paleocene, the oldest and more lasting lateritization event known in Amazon. The mineral composition and distribution suggest a cyclical evolutionary process, with alternating wet and arid conditions, which led to the formation of gibbsite form kaolinite and hematite from goethite, respectively.

Phosphates contents are much lower than other lateritic deposits from Gurupi region, although they are above crustal average. The total conversion of kaolinite to gibbsite occurred only on the aluminous iron crust. The bauxite, however, still presents high contents of kaolinite. The iron a clay (kaolinite) rich profile is very interesting as raw material for cement industry.

ACKNOWLEDGMENTS

The authors would like to thank Vicenza Mineração, which collected and provided the samples; the National Council for Scientific and Technological Development (CNPq) and National Institute of Amazon Geosciences (GEOCIAM) for their financial help; the Ministry of Education (MEC) for the scholarship that was provided to the first author through the Tutorial Education Program (PET); the Federal University of Pará (UFPA), Geosciences Institute; the *Zentrum für Werkstoffanalytik Lauf* (ZWL) for the labor analysis; and Pró-Reitoria de Pesquisa e Pós-Graduação (PROPESP) of UFPA for their financial support.

REFERENCES

Aleva G.J.J. & Creutzberg D. 1994. *Laterites: concepts, geology, morphology and chemistry.* Wageningen, Netherland: International Soil Reference and Information Centre, 169 p.

Amigó J.M., Bastista J., Sans A., Signes M., Serrano J. 1994. Crystallinity of lower cretaceous kaolinites of Teruel. *Applied Clay Science*, **9**(1):51-69.

Aparicio P. & Galán E. 1999. Mineralogical interference on kaolinite crystallinity index measurements. *Clays and Clay Minerals*, **47**(1):2-27.

Bardossy G. 1982. *Karst bauxites.* Amsterdam: Elsevier, 441 p.

Barros A.E., Nardi L.V.S., Dillenburg S.R. 2005. Geoquímica de minerais detríticos em estudos de proveniência: uma revisão. *Revista Pesquisas em Geociências*, **32**(1):3-15.

Calaf J.M.C. 2000. *Evolução geológica no cenozóico da região entre Açailândia (MA) e Ligação (PA).* MS Dissertation, Curso de Pós-graduação em Geologia e Geoquímica, Universidade Federal do Pará, Belém, 122 p.

Costa M.L. 1980. *Geologia, mineralogia, geoquímica e gênese dos fosfatos de Jandiá, Cansa Perna e Itacupim, no Pará, e Pirocaua e Trauíra, no Maranhão.* MS Dissertation, Núcleo de Ciências Geofísicas e Geológicas, Universidade Federal do Pará, Belém, 202 p.

Costa M.L. 1982. *Petrologisch-geochemische Undersuchungen zur Genese der Bauxite und Phosphat-Laterite der Region Gurupi (Ost-Amazonien).* PhD Thesis, Universität Erlangen-Nürnberg, Fakultäten der Friedrich Alexander, Alemanha, 189 p.

Costa M.L. 1990. Mineralogia, geoquímica, gênese e epigênese dos lateritos fosfáticos de Jandiá, na Região Bragantina (NE do Pará). *Geochimica Brasiliensis*, **4**(1):85-110.

Costa M.L. 1991. Aspectos geológicos dos lateritos da Amazônia. *Revista Brasileira de Geociências*, **21**(2):146-160.

Costa M.L. 1997. Lateritization as a major process of ore deposit formation in the Amazon region. *Exploration and Mining Geology*, **6**(1):79-104.

Costa M.L., Cruz G.S., Almeida H.D.F., Poellmann H. 2014. On the geology, mineralogy and geochemistry of the bauxite-bearing regolith in the lower Amazon basin: evidence of genetic relationships. *Journal of Geochemical Exploration*, **146**:58-74.

Costa M.L. & Sá J.H.S. 1980. Os fosfatos lateríticos da Amazonia Oriental: Geologia, Mineralogia, Geoquímica e correlação com as bauxitas da Amazônia. *In:* 31º Congresso Brasileiro de Geologia, Sociedade Brasileira de Geologia, Balneário de Camboriú, Brazil. 179 p.

Delvigne J.E. 1999. *Atlas of micromorphology of mineral alteration and weathering.* Ottawa, Ontario: Mineralogical, Canadian Mineralogist Special Publication 3, 495 p.

Dennen W.H. & Norton H.A. 1977. Geology and geochemistry of bauxite deposits in the lower Amazon basin. *Economic Geology*, **72**(1):82-89.

Du X., Rate A.W., Gee M.A.M. 2012. Redistribution and mobilization of titanium, zirconium and thorium in an intensely weathered lateritic profile in Western Australia. *Chemical Geology*, **330-331**:101-115.

Evensen N.M., Hamilton P.J., O'Nions R.K. 1978. Rare-earth abundance in chondritic meteorites. *Geochimica et Chosmochimica Acta*, **42**(8):1199-1212.

Fitzpatrick R.W. & Schwertmann O. 1982. Al-substitued goethite, an indicator of pedogenic and other weathering environments in South Africa. *Geoderma*, **27**(4):335-347.

Giorgis I., Bonetto S., Giustetto R., Lawane A., Pantet A., Rossetti P., Thomassim J., Vinai R. 2014. The lateritic profile of Balkouin, Burkina Faso: geochemistry, mineralogy and genesis. *Journal of African Earth Sciences*, **90**:31-48.

Hallberg J.A. 1984. A geochemical arid to igneous rock identification in deeply weathered terrain. *Journal of Geochemical Exploration*, **20**:1-8.

Horbe A.M.C. & Costa M.L. 1997. Geoquímica dos ETR no perfil laterítico da Serra do Madeira – Mina do Pitinga, AM. *Geochimica Brasiliensis*, **11**(3):309-324.

Horbe A.M.C. & Costa M.L. 1999. Relações genéticas entre latossolos e crostas lateríticas aluminosas e alumino-ferruginosas na região de Paragominas, Pará. *Revista Brasileira de Geociências*, **29**(4):497-504.

Klein E., Palheta E.S., Pinheiro B.L.S., Moura C.A.V., Abreu F.M. 2005. Sistematização da Litoestratigrafia do Cráton São Luís e do Cinturão Gurupi. *Revista Brasileira de Geociências*, **35**(3):415-418.

Klein E.L. & Moura C.A.V. 2001. Age constraints on granitoids and metavolcanic rocks of the São Luís Craton and Gurupi Belt, northern Brazil: implications for lithostratigraphy and geological evolution. *International Geology Review*, **43**(3):237-253.

Kotschoubey B., Calaf M.J.C., Lobato A.C.C., Leite A.S., Azevedo C.H.D. 2005. Caracterização e gênese dos depósitos de bauxita da província bauxitífera de Paragominas, noroeste da Bacia do Grajaú, nordeste do Pará/oeste do Maranhão. In: Marini O.J., Queiroz E.T., Ramos B.W. (eds.). *Caracterização de depósitos minerais em distritos mineiros da Amazônia.* Brasília, CT-MINERAL/FINEP, ADIMB, p. 691-782.

Leite A.S. 2014. *Geologia, mineralogia e geoquímica dos fosfatos de Sapucaia (Bonito-PA).* MD Dissertation, Programa de Pós-Graduação em Geologia e Geoquímica, Instituto de Geociências, Universidade Federal do Pará, Belém, 111 p.

Liu X., Wanga Q., Zhang Q., Feng Y., Cai S. 2012. Mineralogical characteristics of the superlarge Quaternary bauxite deposits in Jingxi and Debao counties, Western Guangxi, China. *Journal of Asian Earth Sciences*, **52**:53-62.

Mehra O.P. & Jackson M.L. 1960. Iron oxide removal from soils and clays by a dithionite-citrate system buffered with sodium bicarbonate. *Clays and Clay Minerals*, 7(1):317-327.

Oliveira F.S., Varajão A.F.D.C., Varajão C.A.C., Boulangé B., Soares C.C.V. 2013. Mineralogical, micromorphological and geochemical evolution of the facies from the bauxite deposit of Barro Alto, Central Brazil. *Catena*, **105**:29-39.

Oliveira N.P. & Costa M.L. 1984. Os fosfatos aluminosos do Pará e do Maranhão: estágio atual de conhecimentos e estratégia para o aproveitamento econômico. *Ciências da Terra*, **10**:16-19.

Pastana J.M.N. 1995. *Programa Levantamentos Geológicos Básicos do Brasil: Folha Turiaçu/Pinheiro (SA.23-V-D/SA.23-Y-B), estados do Pará e Maranhão.* Texto explicativo. Brasília: Companhia de Pesquisa de Recursos Minerais, 205 p.

Sayin M. & Jackson M.L. 1975. Anatase and rutile determination on kaolinite deposits. *Clays and Clay Minerals*, **23**:437-443.

Thiel V.R. 1963. Zum system α-FeOOH – α-AlOOH. *Zeitschrift Für anorganissche allgemeine Chemie*, **326**(1-2):70-78.

Widepohl K.H. 1995. The composition of the continental crust. *Geochimica et Cosmochimica Acta*, **59**(7):1217-1232.